New Journal of Physics
The open-access journal for physics

Angular encoding in attosecond recollision

Markus Kitzler[1], Xinhua Xie, Stefan Roither, Armin Scrinzi and Andrius Baltuska

Photonics Institute, Vienna University of Technology,
Vienna, Austria
E-mail: markus.kitzler@tuwien.ac.at

New Journal of Physics **10** (2008) 025029 (13pp)
Received 20 September 2007
Published 29 February 2008
Online at http://www.njp.org/
doi:10.1088/1367-2630/10/2/025029

Abstract. We describe a general concept of using the spatial information encoded in the time-dependent polarization of high harmonic radiation generated by orthogonally polarized two-color laser fields. The main properties of recolliding electron wave packets driven by such fields are reviewed. It is shown that in addition to the recollision energy the angle of recollision of such wave packets, which is directly mapped onto the polarization direction of the emitted high harmonic radiation, varies on a sub-laser-cycle time-scale. Thus, a mapping between the polarization angle and the frequency of the emitted radiation is established on an attosecond time scale. While the polarization angle encodes the spatial properties of the recollision process, the frequency is linked to time via the well-known dispersion relations of high harmonic generation. Based on these principles, we show that in combination with polarization selective detection the use of orthogonally polarized drive pulses for high harmonic generation permit one to construct spatially resolved attosecond measurements. Here, we present two examples of possible applications: (i) a method for isolating a single attosecond pulse from an attosecond pulse train which is more efficient than the cut-off selection method, and (ii) a technique for orbital tomography of molecules with attosecond resolution.

[1] Author to whom any correspondence should be addressed.

Contents

1. Introduction

An attosecond electronic wave packet liberated from an atom or molecule by tunnel ionization due to the interaction with a strong laser field preserves its sub-femtosecond temporal structure during the propagation in the laser field and may finally return to the ion as a sub-cycle electron pulse [1, 2]. At the position of the ion the electronic wave packet can interfere with the ground state wavefunction giving rise to photon emission. The spectrum of these photons can be used to probe structure and/or temporal evolution of the ion [3]–[5]. Using this so-called high harmonic spectrum has the advantage over other probing techniques that powerful optical methods such as, e.g., spectral or spatial filtering can be applied. For example, by adequately filtering the spectrum of the emitted radiation it is possible to generate attosecond extreme ultraviolet (XUV) pulses [6, 7]. A spectrum of harmonics arises, because during every half-cycle the impact kinetic energy of the returning electron chirps from low energies to the highest energy of about 3.17 U_p, with U_p being the ponderomotive potential [1]. It was confirmed by a large number of experiments on the sub-laser-cycle chirp of the harmonic spectra, e.g. [8], that the harmonic radiation emitted at any given time can be ascribed to nearly free electrons moving along quasi-classical trajectories and recolliding with the parent system at that time. Therefore control of the trajectories by the laser parameters, i.e. wavelength, pulse duration and pulse intensity, gives control over the properties of the harmonic radiation.

However, wavelength, duration and intensity are not the only parameters to control electron trajectories: laser polarization allows the angular electron motion to be steered. Linearly polarized light restricts the electron motion essentially to the light polarization plane where recollisions and harmonic emission occur nearly continuously over the laser pulse duration. Elliptically polarized fields, on the other hand, take the electron motion into the whole plane orthogonal to laser propagation, where in most cases no recollisions with the parent system will occur. Manipulation of the time-dependent polarization state allows for recollisions to be restricted to a well-defined short time interval. This is exploited, for instance, in the method for single attosecond pulse generation called ‘polarization gating’ [9]–[11]: by using two counter-rotating circularly polarized few-cycle pulses, which are delayed with respect to each other by some appropriate, short time, the ellipticity of the laser field is adjusted such that only during a sub-cycle interval is the laser polarization linear and permits recollision of electrons from the same direction as they were ionized from. At all other times the polarization is elliptical and no recollisions occur.

A completely different recollision scenario arises by the use of orthogonally polarized two color (OTC) pulses. Such pulses consist of two *linearly* polarized laser pulses of two

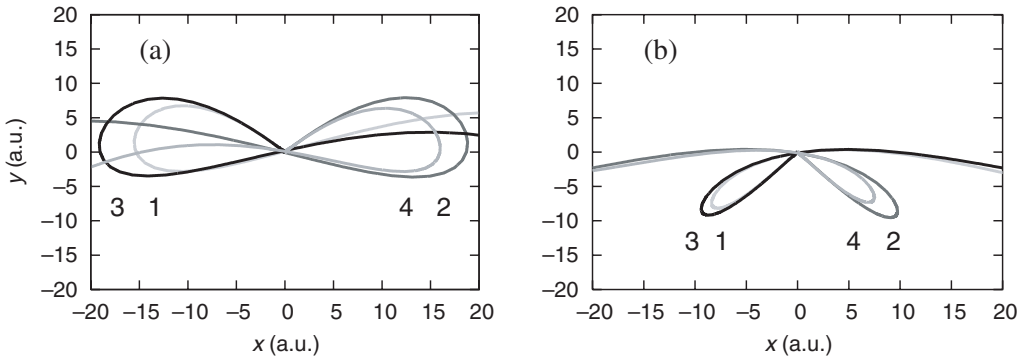

Figure 1. (a) and (b) Typical trajectories of returning electrons in OTC-pulses. The trajectories were calculated by solving Newton's equations for a point charge. Pulse parameters: duration 5 fs (FWHM), Gaussian envelopes, wavelength 790 nm in x, frequency doubled in y, $I_x = I_y = 1.5 \times 10^{14}\,\mathrm{W\,cm^{-2}}$. CE phases: $\phi_{\mathrm{CE},x} = 0$ for (a) and (b), $\phi_{\mathrm{CE},y} = 0.8\pi$ (a), and $\phi_{\mathrm{CE},y} = 1.6\pi$ (b). The numbers of the mean trajectories reflect their sequence of recollision and are used to identify them in the text.

different colors with the fields polarized in two orthogonal directions [12]–[15], whose fields can be described by a vector potential $\mathbf{A}(t)$, from which the electric field can be derived by $\mathbf{E}(t) = -\mathrm{d}\mathbf{A}(t)/\mathrm{d}t$, given by $A_j(t) = -\hat{E}_j(f_j(t)/\omega_j)\sin(\omega_j t + \phi_{\mathrm{CE},j})$. Here $f_j(t)$, $\hat{E}_j$, ω_j and $\phi_{\mathrm{CE},j}$ denote the pulse envelope, peak electric field strength, laser frequency and carrier-envelope (CE) phase, respectively, along the polarization direction $j = \{x, y\}$. Here and for the rest of the paper the pulse peaks are assumed to be at time zero. OTC fields provide formidable freedom for tailoring the recollision process and open up the possibility of steering electronic wave packets with sub-femtosecond precision around the ion core, thereby allowing not only control of recolliding electrons in time but also in space. Figures 1(a) and (b) show typical trajectories of electrons driven by OTC-pulses in the polarization plane. Here, the electrons are treated as point charges and their trajectories are calculated solving Newton's equations. A detailed analysis of the spatial properties of the recolliding electron wave packets shows that the instantaneous recollision direction sweeps over a large range of angles during a short time [12, 16]. The sweep of the electron incidence angle on the parent ion is encoded in the polarization plane of the emitted high harmonics, which as a result rotates rapidly.

With that, in addition to time and high harmonic frequency, which are connected to recollision time and energy, respectively, the *polarization angle* of the harmonic radiation provides a third dimension of observation in a recollision-based experiment. In this paper, we demonstrate that one can exploit the sweep of the polarization of attosecond pulse trains created by OTC few-cycle drive fields in a similar manner as one can make use of the frequency chirp. This is an application of a general concept that is not restricted to harmonic radiation: in the present experiments [5, 6], sub-femtosecond timing information is obtained from the correlation of recollision times with recollision energies. Spatially shaped electron trajectories, cf figure 1, open up the possibility of using the correlation between time and angles in the same manner.

Here, we present two examples of methods that exploit the two-dimensional (2D) spatial character of the emitted radiation. In the first method, the mapping between recollision *time* and *polarization* is exploited for creating short trains of attosecond pulses that can be applied

just as if they were a single attosecond pulse, provided the detection is polarization sensitive. When polarizing XUV optics is used, this method also permits creation of an isolated photonic attosecond pulse with higher efficiency as the cut-off selection method [6]. The second method uses the fact that recollisions occur from different *directions* and with different *energies*. This leads to harmonic emission within a range of angles, which permits single-shot orbital tomography of molecules [3] and, hence, allows orbitals to be traced with sub-cycle resolution as we will explain below.

The paper is organized as follows. Firstly, we will review important properties of the recollision process in OTC fields. Secondly, we will describe how such fields can be applied to create single attosecond pulses, and thirdly, we will explain attosecond tomography using OTC-pulses. We will conclude by summarizing the results of this paper and by giving an outlook on how the unique properties of OTC-pulses could be used for the measurement of centro-symmetric phenomena, possibly on the attosecond time-scale, e.g. ring currents [17] in atoms or molecules, which cannot be measured by linear pulses.

2. The recollision process in orthogonal two-color laser fields

The instantaneous polarization direction of an OTC field varies rapidly on a sub-cycle time-scale. When used as a driving field for electron recollision the two most prominent implications are: (i) the emitted electron wave is driven on trajectories which are ionized in one direction and may return to the ion from another direction. From which direction the trajectory eventually recollides with the ion, if it does at all, sensitively depends on the ratio of the two colors and on their relative phases [13]–[16]. (ii) Because it might happen that the recollision conditions are only fulfilled for parts of the ionized electron wave packet, the temporal structure of the returning electron wave packets is, in general, shorter than in linearly polarized fields [14], where always the entire wave packet returns to the ion. Thus, by choosing appropriate parameters of the OTC field it is possible to exclude parts of the ionized wave packet from recolliding. This is somewhat similar to the technique of polarization gating [9], however, in OTC fields ionization and recollision take place along different directions, in contrast to polarization gating, which makes use of a temporally confined linear polarization. Therefore, polarization gating leads to linearly polarized harmonic light, whereas OTC fields produce harmonic light with a time-dependent polarization direction. This is the basis of the two methods which we will present below.

By adjusting the frequency ratio, the ratio of peak field strengths, which shall be denoted by γ, and the relative phase of the two fields the angle between ejection and return can be controlled. The angle of return with respect to the x-axis of an electron born at t_b which recollides with the ion at time $t_r > t_b$ is given by $\theta_r(t_r, t_b) = \arctan(\dot{y}(t_r, t_b)/\dot{x}(t_r, t_b))$. Within the strong field approximation $\dot{\mathbf{x}}(t_r, t_b) = \mathbf{A}(t_r) - \mathbf{A}(t_b)$, where the electron's initial velocity is neglected. A similar relation can be derived for the angle of ejection: $\theta_b(t) = \arctan(E_y(t)/E_x(t)) = \arctan[\gamma\cos(\omega_y t + \phi_{CE,y})/\cos(\omega_x t + \phi_{CE,x})]$. It was demonstrated that these relations are sufficient to describe the mean values of numerically calculated angle distributions using semi-classical trajectory methods [12].

The instantaneous angle of recollision varies significantly within the short interval of some hundred attoseconds, during which the recollision takes place [12, 16]. For high harmonic generation this means that the polarization of the produced radiation varies with time. This is the basis of the applications we want to discuss below. The reason for this sweep can be

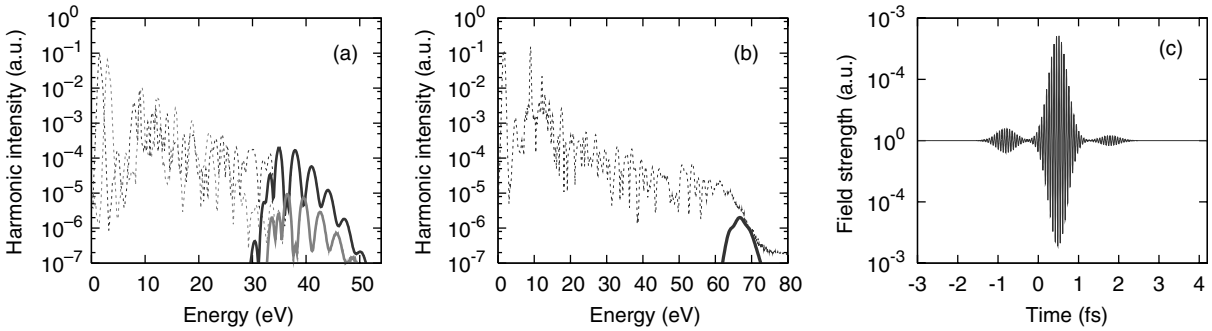

Figure 2. (a) High harmonic spectrum created by an OTC-pulse with the same parameters as in figure 1(a) except for $I_x = I_y = 1.26 \times 10^{14}\,\mathrm{W\,cm^{-2}}$. (b) High harmonic spectrum created by a linearly polarized pulse with the same parameters as the x-component of the OTC-pulse used in (a) but with doubled peak intensity to yield comparable ionization rates. (c) A single attosecond pulse created by cut-off band-pass filtering of the high harmonic spectrum shown in (b) by the thick line. Direction encoding for both panels: dark/light gray lines x/y.

explained using an intuitive picture: similarly to the physics in linearly polarized laser fields, where due to the well-known dispersion relation of high harmonic generation [1] parts of the electronic wave packets ionized at different times within a half-cycle, returning to the ion with much different energy, in the 2D laser fields of OTC-pulses those parts of the wave packets additionally recollide with the ion under different angles: tiny differences in ionization time are mapped onto huge differences in recollision energies and angles by the laser field. Whereas the different return energies result in a chirp of the instantaneous electron momentum, which translates into a broad spectrum in the frequency domain, the different return angles translate into a sweep of the instantaneous recollision angle. Note, that both chirp and sweep are governed by the field on a sub-cycle time-scale. Consequently, high harmonics created by OTC-pulses will not only be emitted in a short burst, but also their polarization will rotate rapidly within the laser pulse.

3. Production of single attosecond pulses

Now, we discuss the application of OTC drive pulses for the generation of single attosecond pulses. For a quantitative comparison of the efficiency with the conventional cut-off band-pass filtering method used for linearly polarized pulses [6] we have numerically solved the time-dependent Schrödinger equation in 2D for one electron in a shielded Coulomb potential. The shielding parameter was adjusted to yield the ionization potential of argon. Figures 2(a) and (b) show high harmonic spectra created with orthogonal two-color and linear light, respectively. The linearly polarized pulse has the same parameters as the x-component of the two-color pulse except that we have doubled the peak intensity to ensure comparable maximum vectorial field strengths and ionization rates.

A 3D representation of the pulse train created by the OTC-pulse—after filtering away the low harmonics but otherwise leaving the spectrum unchanged, see figure 2(a)—is shown in figure 3 by the black line. The three pulses correspond to three recolliding wave packets

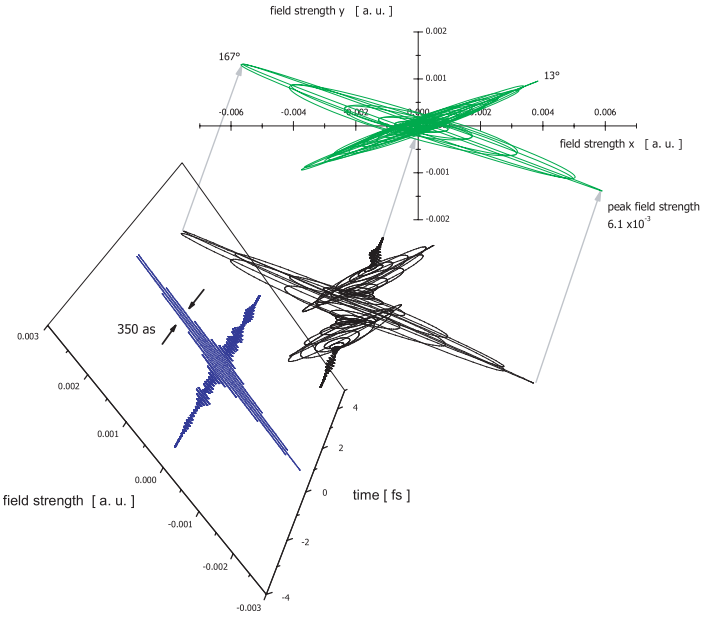

Figure 3. 3D representation of the pulse train whose spectrum is shown in figure 2(a) after high-pass filtering as indicated in figure 2(a) by the thick lines. The blue line shows a projection as yielded by a polarizer of the 3D field onto a plane orthogonal to the double pulse structure. This way only the single attosecond pulse with a polarization direction of 167° is selected. The green line at the back shows a projection of the 3D field along the time axis onto the xy-plane.

whose mean trajectories are depicted in figure 1(a) in the xy-plane, numbered 1, 2 and 3. The returning trajectory number 4 returns to the ion with little kinetic energy and is thus filtered away with the low harmonics. To isolate a single attosecond pulse from a pulse train produced by linearly polarized driving light one usually reflects the radiation off a metallic multi-layer mirror with a reflectivity of about 70%, which acts as an almost Gaussian spectral filter [6], thereby selecting only the highest energetic harmonics, called the cut-off. These harmonics correspond to a single recolliding trajectory and therewith to a single attosecond pulse, cf figure 2(c). This pulse was created by shifting a Gaussian filter, see black line in figure 2(b), to higher energies until only one pulse remained. The width of the filter was adjusted to minimize the amplitude of the pre-pulse. When filtering out the cut-off harmonics, only a tiny fraction of the whole high harmonic spectrum is used, which strongly reduces the pulse's field strength, as discussed below. By contrast, in the proposed OTC-configuration one can use polarization selective detection to suppress the extra peaks. For the pulse parameters assumed in figures 1(a) and 2(a), two of the three contributing trajectories recollide under the same angle, while the third one returns from a distinctly different direction, cf trajectories numbers 1 and 3 versus number 2 in figures 1(a) and (b). This effectively results in three attosecond pulses, where two are polarized in the same and one is polarized in another plane. The mixed polarization state of such a pulse train can immediately be used to obtain a single attosecond XUV pulse, when the pulse train is reflected off a metallic multi-layer mirror, as described above. For larger incidence angles such mirrors exhibit almost ideal polarizing properties in this wavelength regime [18], even for broadband radiation of up to 20 eV bandwidth [19]. The results of such a polarization

selection are demonstrated in figure 3 by the blue line, where the the effect of a polarizer is simulated by projecting the 3D harmonic field onto a plane orthogonal to the polarization plane of the double pulse structure created by the recolliding trajectories numbers 1 and 3. This way the harmonic pulses created by these two trajectories are suppressed and only the pulse created by trajectory number 2 recolliding under -13° to the x-axis is selected. Consequently, the polarization selection results in a single photonic attosecond pulse.

For most experimental applications, however, one can avoid the use of a multi-layer mirror by instead detecting photo-electrons or ions in a selected plane, e.g. in our example $-13^\circ \equiv 167^\circ$ to the x-axis. Such a detection does not rely on projections, as is the case with polarizing optics, but effectively results in cuts along a certain direction in the xy-plane. As can be seen in figure 3, by comparing the peak value of the blue pulse with that of the 3D pulse (shown in green in the coordinate system in the back), the peak field strength along the -13°-direction is by more than a factor of two higher than that of the projected pulse. Therefore the achievable intensity is approx. a factor of 5 higher. Additionally, the losses due to the reflection off the polarizing multi-mirror are avoided. Thus, an equivalent single attosecond pulse-response at a much higher peak intensity on target is obtained.

Further, we note that for identical values of peak drive field strengths, maximum ionization rates and pulse envelopes chosen for figure 2, the efficiency of a single attosecond pulse production by polarization selection via a polarizer is higher compared to cut-off selection (1 order of magnitude in intensity), cf figure 2(c) with the blue pulse in figure 3, although the carrier frequency of the pulse created by the OTC drive pulse is lower. The peak efficiency with $\omega + 2\omega$ OTC-pulses is reached at $\Delta\phi = \phi_{\mathrm{CE},x} - \phi_{\mathrm{CE},y} = -0.8\pi$ (recollision in OTC-pulses sensitively depends on $\Delta\phi$). The reason for the difference in efficiency of the two methods is that for polarization selection a broad spectral range in the plateau can be used, because only a pulse train needs to be generated. For cut-off selection only a narrow spectral band in the cut-off can be used. In addition, the spectral intensity in the cut-off is typically 1–2 orders of magnitude lower than in the plateau.

Therefore, finally, the overall achievable gain in intensity when comparing the cut-off selection method with the OTC-pulse train in combination with angular photo-electron/ion detection is roughly a factor of 60.

4. Attosecond tomography

In the remainder of this paper, we discuss the feasibility of another application of polarization selective detection of high harmonics generated by OTC-pulses: attosecond orbital tomography. In [3], 'molecular orbital tomography' was introduced, where the orbital from which an electron becomes detached by laser ionization is reconstructed from the emitted harmonic spectra. The method of orbital tomography is based on the observation that the spectral intensity of harmonic emission, which can be described by the bound–continuum dipole transition matrix element $\mathbf{d}(\mathbf{k})$, is dominated by a Fourier transform of $\mathbf{x}\Psi_g(\mathbf{x})$, with $\Psi_g(\mathbf{x})$ being the wavefunction of the orbital under consideration: $\mathbf{d}(\mathbf{k}) = a(\mathbf{k})\langle\Psi_g(\mathbf{x})|\mathbf{x}|\exp(\mathrm{i}\mathbf{k}\mathbf{x})\rangle$. The pre-factor $a(\mathbf{k})$ is the quantum mechanical amplitude of the recolliding electron wave packet in Fourier space. When it can be determined by comparing to a known, e.g. atomic system [3], analyzing the harmonic radiation provides a Fourier transform of $\mathbf{x}\Psi_g(\mathbf{x})$.

The procedure on how to correctly extract the information about the orbital from the harmonic spectra is currently a point of discussion. It was shown that the shape of the

continuum wavefunction and the gauge used for describing the recombination term are of crucial importance [20, 21]. Also multi-electron effects influencing recombination cannot be neglected, e.g. [22]. Furthermore, it was shown [23, 24] that using existing theories for molecular ionization [25] to adjust the angular dependence of ionization in molecules and atoms does not always lead to correct results. Here, we do not debate specific problems of the reconstruction procedure. In the description below, we only rely on fully numerical results without resorting to the strong field approximation. Rather, the focus of our discussion lies on a series of fundamental limitations of the originally proposed measurement procedure which all have their origin in using linearly polarized light for recording the high harmonic spectrum: with linear polarization, the direction of electron recollision and with it the wave vectors **k** remain restricted parallel to the polarization direction. In that case, it is unavoidable to perform a set of XUV spectral measurements in multi-shot mode for a range of alignment angles of the molecules relative to the recollision direction, i.e. relative to the laser polarization, for a complete 3D image of the orbital. Although the necessity for many measurements per reconstruction is inconvenient, there are still more fundamental disadvantages of the multi-shot method: (i) because a high harmonic spectrum has to be measured for every relative angle of a molecule to the laser polarization direction, only snapshots temporally integrated over the whole drive pulse duration can be recorded. Since even the shortest pulses have a duration of approx. 4–5 fs, it is inherently impossible to reach the attosecond time domain. (ii) Since it is necessary to align the molecule under study relative to the laser polarization direction, only molecules with a pronounced polarizability axis can be imaged. (iii) Linear polarization is blind to time-dependent centro-symmetric phenomena, such as, e.g., electronic ring currents [17], because every projection would look the same.

In contrast to the linear polarization approach, it is possible to use OTC-pulses for a single-shot measurement which allows reconstruction of the bound orbital within a single cycle of the fundamental driving field. A limit to the temporal resolution is only set by the desired spatial resolution. The reason for the attosecond resolution is that the recollision energy and the recollision angle are chirped within a single sub-femtosecond pulse of the emitted harmonic radiation and as a consequence the whole range of possible angles is covered during two recollisions. This is a direct consequence of the fact that the relation between the angles of ionization and recollision on the one hand, and these angles and the recollision energy on the other hand is established by the driving OTC field.

The quality of a tomographic reconstruction is determined by the quantum mechanical amplitude of the recolliding electron wave packet in Fourier space, $a(\mathbf{k})$. If it matches the extension of the orbital to the image in Fourier space, all momentum components are covered and the orbital can be retrieved by a Fourier transform; provided $a(\mathbf{k})$ can be determined from a reference system. Using a semi-classical treatment of the recollision wave packets it was shown recently [16] that it is possible to cover the Fourier space in a single shot by using OTC drive pulses. Here, we perform a fully quantum mechanical calculation of $a(\mathbf{k})$ by solving the time-dependent Schrödinger equation in 2D numerically exact.

An important difference between orthogonal two-color single-shot and linearly polarized multi-shot tomography is that different areas in the Fourier space are covered. Because of the aforementioned relation between the angle of recollision and the recollision energy in the single-shot version, the total probability returning to the ion is spread out over a range of angles, which entails a loss of resolution for each single angle. By comparing the coverage of the Fourier space through $a_{\mathrm{OTC}}(\mathbf{k})$ of an OTC-pulse with the parameters as indicated in figure 2, except

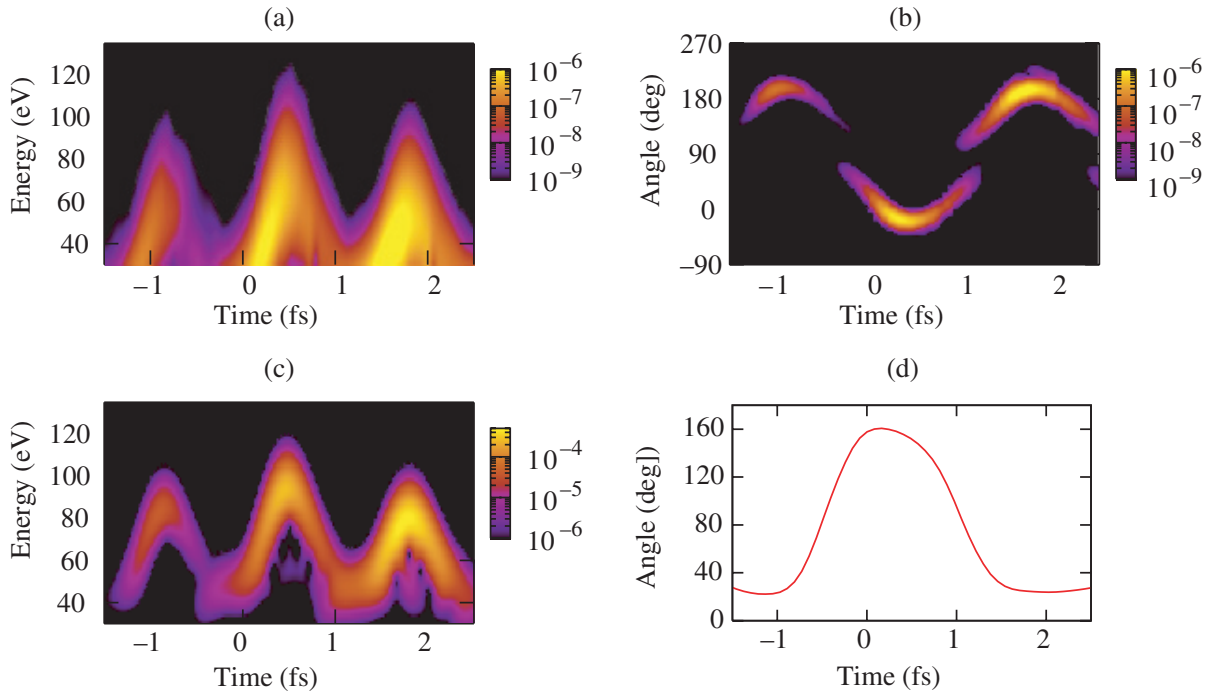

Figure 4. Probability density functions of recollision energy (a) and angle (b) over time. (c) Time–frequency plot of the dipole response of an atomic model as defined in the text. (d) Polarization angle of the emitted harmonic radiation over time. The recollision energy in (a) is plotted with the ionization potential added to be directly comparable to the harmonic energy plotted in (c). The parameters of the OTC-pulse are the same as in figures 2(a) and 3 except for peak intensity $I_x = I_y = 3.5 \times 10^{14}\,\mathrm{W\,cm^{-2}}$.

for a higher peak intensity of $I_x = I_y = 3.5 \times 10^{14}\,\mathrm{W\,cm^{-2}}$, to the coverage obtained with a comparable linear pulse, we demonstrate that in spite of the lower resolution, the single-shot measurement yields the main characteristics of the orbital.

To simplify the discussion, we study the image of the wavefunction $\Psi_g(\mathbf{x})$ rather than $\mathbf{x}\Psi_g(\mathbf{x})$; the former can be reconstructed from the latter everywhere except near the origin [3]. The wavefunction in momentum space is denoted by $\Phi_g(\mathbf{k}) = \langle \Psi_g(\mathbf{x}) | \exp(\mathrm{i}\mathbf{k}\mathbf{x}) \rangle$. We discuss the case of a diatomic molecule with its molecular axis aligned close to 50° relative to the x-axis of the two-color field. This can be achieved either by a separate aligning pulse or even without extra alignment by the preponderance of ionization for parallel alignment [25], when the peak field points in that direction (cf figure 1).

In the following we will derive the inversion map $a(\mathbf{k})$ as well as probability density functions for recollision energy and recollision angle from the wavefunction $\Psi(x, y; t)$ computed by solving the Schrödinger equation. These quantum mechanical functions can be directly compared to classically calculated values [12, 16]. They also facilitate a comparison with the emitted high harmonic radiation and therewith with the 3D attosecond pulse train discussed in the previous section. Figures 4(a) and (b) show the probability density functions of energy and angle over time of the recolliding wave packets in the OTC-pulse, respectively. The kinetic recollision energy is plotted here with the ionization potential added in order

to be directly comparable to the harmonic power spectrum shown in figure 4(c) below. The angle of the polarization plane of the harmonic radiation over time is plotted in figure 4(d), which follows the recollision angle of the wave packets shown in figure 4(b). Please note, the polarization angle is defined in the interval $[0, \pi]$ and therefore, e.g., $167^\circ \equiv -13^\circ$. Since here the same parameters of the OTC-pulse as in figure 3 were used, the angle of the polarization plane can be compared to that of the harmonic pulse shown there. Likewise the recollision angle shown in figure 4(b) can be compared to the recollision angle of the classical trajectories shown in figure 1(a), which were calculated using purely classical relations with the electrons treated as point charges. The probability densities in figures 4(a) and (b) were derived from the numerically propagated 2D wavefunction by Fourier transforming it to momentum space after applying 2D Gaussian mask functions at some small distances from the ion [26]. The mask functions $g(\mathbf{r}_0; w)$, with $\mathbf{r}_0 = (r_0, \theta)$ and w being the vector from the position of the ion to the center of the mask functions and the width of the mask functions, respectively, cut out pieces of the total wavefunction, $\Psi(x, y; t)$, sufficiently far away from the ion to only mask the free wave packet, but close enough such that the parameters of the wave packet at position $\mathbf{r}_0$ equal those at the ion's position [26]. Masking the wavefunction yields a number of functions $\Phi^\theta(x, y; t) = \Psi(x, y; t)\, g(\theta)$, one for every mask function defined by the parameter θ. Here, we have dropped the parameters r_0 and w for the sake of simplicity, since they are the same for every piece of the masked wavefunction $\Phi^\theta(x, y; t)$. A transformation of the masked functions to Fourier space yields $\tilde{\Phi}^\theta(k_x, k_y; t) \equiv \tilde{\Phi}^\theta(k_\parallel, k_\perp; t)$, with the parallel and perpendicular directions defined with respect to the vector $\mathbf{r}_0$. The probability density function $P(E_\mathrm{k} + I_\mathrm{p}, t)$ of the kinetic recollision energy E_k over time shown in figure 4(a) is then derived from $\tilde{\Phi}^\theta(k_\parallel, k_\perp; t)$ by summing up all contributions from the various θ and making use of $E_\mathrm{k} = k_\parallel^2/2$, $P(E_\mathrm{k} + I_\mathrm{p}, t) = |\sum_\theta \tilde{\Phi}^\theta(\sqrt{2E_\mathrm{k}} + I_\mathrm{p}, t)|^2$, where $k_\perp$ was integrated over a small interval $[-k_\perp^0, +k_\perp^0]$, with $k_\perp^0$ such that the wave packet within this interval hits the origin, and the ionization potential I_p was added in order to facilitate a direct comparison of $P(E_\mathrm{k} + I_\mathrm{p}, t)$ with the high harmonic power spectrum shown in figure 4(c). The probability density function $Q(\theta, t)$ of the recollision angle θ over time shown in figure 4(b) is likewise derived from $\tilde{\Phi}^\theta(k_\parallel, k_\perp; t)$ by integrating over all $k_\parallel$ and $k_\perp$ in the interval $[-k_\perp^0, +k_\perp^0]$. The time frequency plot of the harmonic radiation shown in figure 4(c) is calculated by performing a windowed Fourier transform of the dipole acceleration, and the polarization angle of the harmonic radiation over time shown in figure 4(d) is computed by averaging over the fast oscillations of the instantaneous electric field's polar angle within the duration of the applied time window.

Finally, in order to calculate the recollision amplitude $a_\mathrm{OTC}(\mathbf{k}) \equiv a_\mathrm{OTC}(k_\parallel, \theta)$, shown in figure 5(a), the function $\tilde{\Phi}^\theta(k_\parallel, k_\perp; t)$ is integrated over time t and $k_\perp$, again only within the range of perpendicular momenta $[-k_\perp^0, +k_\perp^0]$, and taking the absolute square of the integrated function. The similarity to the semi-classically calculated $a_\mathrm{OTC}(\mathbf{k})$ of [16] is striking, thus justifying the semi-classical approach.

In the reconstruction of the bound wavefunction via the inverse Fourier transform $\Psi^\mathrm{OTC}_{g,\mathrm{rec}}(\mathbf{x}) = \langle \exp(\mathrm{i}\mathbf{k}\mathbf{x}) | a_\mathrm{OTC}(\mathbf{k}) \Phi_g(\mathbf{k}) \rangle$ the recollision amplitude $a_\mathrm{OTC}(\mathbf{k})$ acts as if the wavefunction is sampled in these momentum regions only, where $a_\mathrm{OTC}(\mathbf{k})$ is significant for a given noise-to-signal ratio. In our reconstruction, we only considered regions where the probability was not more than 2 orders of magnitude below the maximum value, all other regions were set to zero. The probability within the contributing regions can be set to 1, since for the orbital reconstruction method it is assumed that the probability amplitude $a(\mathbf{k})$

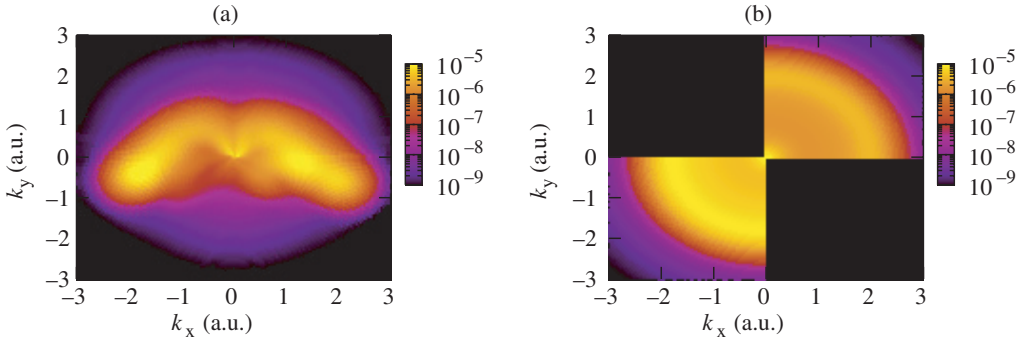

Figure 5. (a) Inversion map $a_{\mathrm{OTC}}(\mathbf{k})$ in momentum space as defined in the text calculated for an OTC-pulse with the parameters as in figure 2. (b) Multi-shot inversion map $a_L(\mathbf{k})$ created by the linearly polarized pulse used in figure 2(b) but with $I = 3.5 \times 10^{14}\,\mathrm{W\,cm^{-2}}$, when the polarization is deliberately rotated over a full quadrant $(\pi/2)$.

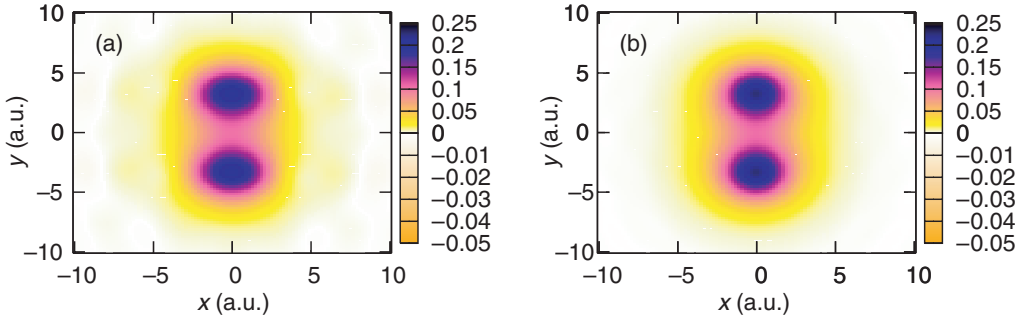

Figure 6. Reconstructed ground state wavefunction using the two-color (a) and the multi-shot (b) inversion maps of figure 5. In both cases the known axial symmetry of the molecule was exploited for the inversion. For the parameters used here the reconstruction using the multi-shot inversion map is almost a perfect one. Thus, (b) is equal to the exact ground state within the resolution of the picture. Note the expanded scale for the negative values in the color coding.

can be acquired by a separate measurement [3]. In addition, we make use of the known axial symmetry of the wavefunction. The resulting reconstructed wavefunction $\Psi^{\mathrm{OTC}}_{g,\mathrm{rec}}(\mathbf{x})$ is shown in figure 6(a). We compare the reconstructed wavefunction received with the OTC-pulse to the reconstructed wavefunction using linearly (L) polarized light, $\Psi^{L}_{g,\mathrm{rec}}(\mathbf{x})$, which is shown in figure 6(b). Both reconstructed wavefunctions in figures 6(a) and (b) were rotated into the y-axis for easier comparison. The 2D amplitude for linear polarization, figure 5(b), is obtained by rotating the 1D function $a_{\mathrm{L}}(k_{\parallel})$ through a range of angles $[0, \pi/2]$. $a_{\mathrm{L}}(k_{\parallel})$ is calculated in the same way as $a_{\mathrm{OTC}}(k_{\parallel}, \theta)$, and the reconstruction is again performed as described above, once more exploiting the axial symmetry of the wavefunction. The smaller energy range and angular inhomogeneity of a_{OTC} as compared to a_{L} account for the slightly poorer reconstruction, cf figure 6(a) versus (b).

5. Conclusion and outlook

In summary, using an exact numerical solution of the time-dependent Schrödinger equation, we have demonstrated two examples of coherent measurement methods which are based on the polarization sweep of harmonic radiation created by such fields. The first example is creation of high harmonic attosecond pulse trains which can be used just as if they were a single attosecond pulse. Figures 4(c) and (d) show energy and polarization of such a pulse train over time. Clearly, there is only one pulse polarized at $\approx 167^\circ$, which can be selected by either a polarizing element or simply by using its effects in angularly selective photo-electron/ion detection. The second example is a method to perform molecular tomography in a single shot. The crucial measure for the quality of the tomographic reconstruction is the coverage of the momentum space extension of the bound wavefunction under study by the recolliding electronic wave packets. By computing the inversion map, we have shown that it is possible to achieve this coverage in a single shot, cf figure 5(a). The inversion map is a time-integrated picture of the recolliding wave packets, whose energies and angles are depicted in figures 4(a) and (b), respectively.

Figure 4 not only demonstrates that the created high harmonic radiation almost exactly mirrors the properties of the recolliding wave packets but also that the angular sweep as well as the energy chirp of the recolliding wave packets are linked by the driving field on an attosecond timescale: during one half-cycle of the driving field the energy chirps up to a maximum and down to zero (as in linearly polarized laser fields) (figure 4(a)). But during the same time the recollision angle sweeps over a full quadrant (figure 4(b)). In the next half-cycle the energy chirps again up and down and this time the angle sweeps over another quadrant. Thus, a sweep over 180° is performed every cycle of the field, and for molecules exhibiting axial symmetry, a full tomographic reconstruction of the bound state wavefunction will be possible within a single cycle of the driving field. In many applications, however, for example to trace the position of a rotating electron wave packet, it might be sufficient to record the high harmonic radiation in a given angular interval, which can be performed in a fraction of a half-cycle. Therefore polarization selective detection will open a way to a new class of experiments: tracing electron dynamics in molecules with attosecond resolution coherently in space, energy and time by all-optical measurements.

Experimentally, tracing $\Phi_g(\mathbf{k})$ with sub-cycle resolution requires a temporally, spectrally and angularly resolved measurement of the harmonic intensity. This is possible by the linear technique of coherent dual-channel spectral interferometry [27], with a fully characterized linearly polarized XUV pulse [28] as the reference: the harmonic radiation together with the delayed reference pulse is split into two beams; reflection off a polarizing metallic multi-layer mirror for each of the beams and a subsequent spectral analysis yields, together with the known spectral phase of the reference pulse, two orthogonal projections of the harmonic *field*, which is the complete information one can obtain from a high harmonic generation experiment. Therefore, we emphasize that such an implementation of attosecond tomography would also yield the *phase* of the re-constructed orbital, so far experimentally inaccessible [3].

Acknowledgments

We acknowledge fruitful discussions with D Kartashov, U Kleineberg and G Reider. This work was financially supported by the Austrian Science Fund, grants SFB016 and U33-16, and the EURYI award scheme (http://www.esf.org/euryi).

References

[1] Corkum P 1993 Plasma perspective on strong-field multiphoton ionization *Phys. Rev. Lett.* **71** 1994
[2] Corkum P B and Krausz F 2007 Attosecond science *Nat. Phys.* **3** 381
[3] Itatani J *et al* 2004 Tomographic imaging of molecular orbitals *Nature* **432** 867
[4] Niikura H, Villeneuve D M and Corkum P B 2005 Mapping attosecond electron wave packet motion *Phys. Rev. Lett.* **94** 083003
[5] Baker S *et al* 2006 Probing proton dynamics in molecules on an attosecond time scale *Science* **312** 424
[6] Kienberger R *et al* 2004 Atomic transient recorder *Nature* **427** 817–21
[7] Paul P *et al* 2001 Observation of a train of attosecond pulses from high harmonic generation *Science* **292** 1689–692
[8] Salières P *et al* 2001 Feynman's path-integral approach for intense-laser–atom-interactions *Science* **292** 902
[9] Corkum P, Burnett N and Ivanov M 1994 Subfemtosecond pulses *Opt. Lett.* **19** 1870
[10] Sola I *et al* 2006 Controlling attosecond electron dynamics by phase-stabilized polarization gating *Nat. Phys.* **2** 319–22
[11] Sansone G *et al* 2006 Isolated single-cycle attosecond pulses *Science* **314** 443–6
[12] Kitzler M and Lezius M 2005 Spatial control of recollision wave packets with attosecond precision *Phys. Rev. Lett.* **95** 253001
[13] Kim I J *et al* 2005 Highly efficient high-harmonic generation in an orthogonally polarized two-color laser field *Phys. Rev. Lett.* **94** 243901
[14] Kim C M *et al* 2005 Generation of a strong attosecond pulse train with an orthogonally polarized two-color laser field *Phys. Rev.* A **72** 033817
[15] Kitzler M, O'Keeffe K and Lezius M 2006 Attosecond control of electronic motion using light wave synthesis *J. Mod. Opt.* **53** 57
[16] Kitzler M *et al* 2007 Optical attosecond mapping by polarization selective detection *Phys. Rev.* A **76** 011801
[17] Barth I *et al* 2006 Unidirectional electronic ring current driven by a few cycle circularly polarized laser pulse: quantum model simulations for Mg-porphyrin *J. Am. Chem. Soc.* **128** 7043
[18] Schulze D *et al* 1998 Polarization of the 61st harmonic from 1053-nm laser radiation in neon *Phys. Rev.* A **57** 3003
[19] Kleineberg U 2007 private communication
[20] Ciappina M F, Chirilă C C and Lein M 2007 Influence of Coulomb continuum wave functions in the description of high-order harmonic generation with H_2^+ *Phys. Rev.* A **75** 043405
[21] Kamta G L and Bandrauk A D 2005 Three-dimensional time-profile analysis of high-order harmonic generation in molecules: nuclear interferences in H_2^+ *Phys. Rev.* A **71** 053407
[22] Patchkovskii S *et al* 2006 High harmonic generation and molecular orbital tomography in multielectron systems: beyond the single active electron approximation *Phys. Rev. Lett.* **97** 123003
[23] Pavičić D *et al* 2007 Direct measurement of the angular dependence of ionization for N_2, O_2, and CO_2 in intense laser fields *Phys. Rev. Lett.* **98** 243001
[24] Kamta G L and Bandrauk A D 2006 Imaging electron molecular orbitals via ionization by intense femtosecond pulses *Phys. Rev.* A **74** 033415
[25] Tong X, Zhao Z and Lin C 2002 Theory of molecular tunneling ionization *Phys. Rev.* A **66** 033402
[26] Xie X *et al* 2007 Time and momentum distributions of rescattering electrons *J. Mod. Opt.* **54** 999
[27] Walecki W *et al* 1997 Characterization of the polarization state of weak ultrashort coherent signals by dual-channel spectral interferometry *Opt. Lett.* **22** 81
[28] Mairesse Y and Quéré F 2005 Frequency-resolved optical gating for complete reconstruction of attosecond bursts *Phys. Rev.* A **71** 011401